Study of Downward Gas Jets into a Liquid

Ahad Emami and Cedric Briens
Dept. of Chemical and Biochemical Engineering, The University of Western Ontario, London, Ontario, Canada N6A 5B9

DOI 10.1002/aic.11524
Published online July 11, 2008 in Wiley InterScience (www.interscience.wiley.com).

Gas jet penetration is an important factor in gas distributor design for two- and three-phase reactors. The penetration length of downward nonreacting gas jets was measured in liquid by optical method and for gas jet velocities at subsonic conditions. The effects on jet penetration of nozzle diameter, gas density, gas jet velocity, liquid viscosity, and liquid surface tension were examined. A generalized correlation to predict the penetration depth of downward gas jets was obtained. Also a simple model, using a shell momentum balance and assuming downward gas jet as a downward cone with constant angle, was introduced and validated with experimental data. Bubble size calculated based on gas jet fluctuation frequency and validated by high-speed videos.
 AIChE J, 54: 2269–2280, 2008
Keywords: downward gas jet, jet penetration length, jet fluctuation frequency, bubble size, gas liquid, modeling

Introduction

Knowledge of gas jet penetration is vital for the design and operation of spargers used in slurry bubble columns. Many bubble columns are equipped with sparger gas distributors with downward facing holes. If the sparger is too close to the bottom of the column, there may be excessive erosion/corrosion. If it is not close enough, stagnant zones will form, which may lead to undesirable by-products, the formation of hot spots and coking. These potential problems are even more serious with slurry bubble columns. Emami and Briens (2003)[1] showed how the optimum height of a downward sparger could be determined in slurry bubble columns. Most of the gas jet penetration studies have been performed in gas–solid systems, with some studies of gas jet penetration in molten metals related to the steel making process. The gas jet penetration length in gas–solid fluidized beds has received a great deal of attention in the literature (for example, Merry, 1971[2], 1975[3]; Musmarra, 2000;[4] Okhotskii, 2001;[5] Vaccaro, 1997;[6] Vaccaro et al., 1997;[7] Zenz, 1968)[8]. Design of gas grids and spargers must be improved to reduce erosion of reactor internals catalyst attrition and forming the defluidized zones in chemical reactors including two-phase and three-phase reactors. In gas–liquid systems there have been few studies. Kerney et al. (1972)[9] studied the penetration length of a horizontal submerged steam jet in choked conditions in a subcooled liquid water bath by photography technique. Flat head and conical nozzles were used. Their inner tip diameter was in the range of 1.58–9.50 mm. Kerney et al. (1972)[9] assumed that the condensation process takes place at the gas–liquid interface and that it is limited by the rate of heat transfer from the gas–liquid interface to the bulk of the liquid. They provided the following equation:

$$\frac{2L_{\text{jet}}}{d} = \frac{1}{1.932}\,\frac{h_{\text{fg}}}{C_{\text{p}}(T_{\text{s}} - T_{\infty})}\left(\frac{G_{\text{tip}}}{G_{\text{m}}}\right)^{0.5}, \qquad (1)$$

where L_{Jet} is the gas jet penetration length, d is nozzle diameter, h_{fg} is heat of vaporization of liquid, C_{p} is liquid specific heat, G_{tip} is gas mass flux at nozzle tip, G_{m} is average mass flux at gas liquid interface, T_{s} and T_{∞} are steam and liquid bath temperature, respectively. Carreau et al. (1986)[10] photographed a horizontal sonic gas jet submerged in water. The nozzle diameter was 0.3–1 mm and the upstream pressure was 1–10 MPa. They used nitrogen gas in water at 288 K.

Correspondence concerning this article should be addressed to C. Briens at cbriens@uwo.ca.

The mean jet angle, as measured by photography technique, was 25° and independent of applied pressure (0.5–10 MPa). They used a specific type of modified Froude number to correlate the jet penetration length.

$$Fr^* = \frac{\rho_{tip} u_{tip}^2 + (P_{tip} - P_{atm})}{g(\rho_l - \rho_g)d} \tag{2}$$

$$\frac{L_{jet}}{d} = 1.34(Fr^*)^{0.39}, \quad Fr^* < 10^5 \tag{3}$$

where P_{tip} and P_{atm} are pressures at the nozzle exit and in the surrounding fluid, respectively, and ρ_{tip} is the gas density at the nozzle exit. ρ_l and ρ_g are liquid- and gas-phase densities. u_{tip} is the gas velocity at nozzle tip.

Hoefele and Brimacombe (1979)[11] gave the following equation for horizontal gas jets for the air/water system.

$$\frac{L_{jet}}{d} = 10.7 Fr^{0.46} \left(\frac{\rho_g}{\rho_l}\right)^{0.35} \tag{4}$$

where $Fr = \frac{\rho_g u_{tip}^2}{\rho_l g d}$ is the modified Froude number.

Davidson (1990)[12] used the free jet velocity profile and assumed a sharp gas/liquid interface for downward normal and swirling jets. The following relationship between the penetration length of a nonswirling gas jet and the modified Froude number can be extracted from his results:

$$\frac{L_{jet}}{d} = 1.5 \left(\frac{u_{tip}^2}{gd} \frac{\rho_g}{\rho_l - \rho_g}\right)^{0.5} \tag{5}$$

Kozlowski and Wraith (1986)[13] studied the cavity of a downward gas jet injected in liquid phase very close to the wall of a liquid tank. They recorded the gas envelope by high-speed cinematography at framing rate of 150–500 s^{-1}. Nozzle diameters were 4.62, 5.62, and 9.62 mm for two dimensional experiments and 5.37 mm for a three dimensional one. The following expression was derived based on Schlichting velocity equation:

$$\frac{L_{j,max}}{d} = 2.78 \left(\frac{u_{tip}^2}{gd} \frac{\rho_g}{\rho_l}\right)^{1/3} \tag{6}$$

As one can see from the literature, there were only two publications on vertical jets in liquids. Only one publication reported on the effect of gas density on jet penetration and none reported on the effect of liquid properties, for example, surface tension and viscosity. Moreover, although gas jets fluctuate, their fluctuation behavior was not studied. Finally, using cinematography for measurements makes it difficult to accurately measure the fluctuating behavior of the jets and to get a good statistical average of the jet penetration depth.

This article, therefore, presents the results of a study of the penetration of downward gas jets in liquids, which used both cinematography and a more convenient and accurate measurement method. The effects of gas and liquid properties are reported.

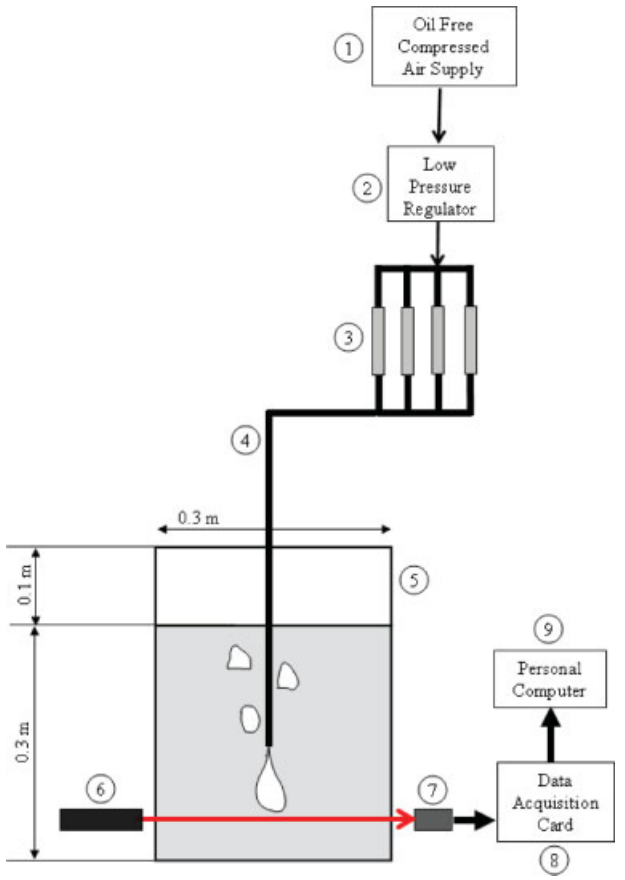

Figure 1. Schematic diagram of the experimental setup.

1: Oil free compressed air supply, 2: Low pressure regulator, 3: Sonic nozzles, 4: Single jet nozzle, 5: Rectangular tank, 6: Laser source, 7: Photodiode cell, 8: National Instrument data acquisition card, 9: Personal computer. [Color figure can be viewed in the online issue, which is available at www.interscience.wiley.com.]

Experimental Setup and Procedure

A schematic diagram of experimental setup is shown in Figure 1. All experiments were performed at room temperature (20–22°C) and in a rectangular glass tank with dimension of 0.6 m length, 0.3 m width, and 0.4 m height which was filled up to 75% of its height with different liquids such as distilled water, ethanol (95%), or sucrose solutions, to vary the liquid viscosity and surface tension. Helium, argon, and oil-free air were used as gas phase. Gas mass flow rate for helium was unto 0.15 g/s and for air and argon were 1.1 and 1.3 g/s, respectively. The gas was introduced into the liquid through a submerged downward stainless steel tube. Four nozzle diameters were used. The inner diameters of the nozzles were 1.07, 2.03, 2.85, and 4 mm. The length of stainless steel tube was 0.7 m.

A battery of four, calibrated sonic nozzles, supplied by a pressure regulator, was used to control and monitor the gas mass flow rate. Gas velocity was low enough that the flow can be assumed as an incompressible flow (Ma < 0.3) for the most of experimental conditions (Table 1). Nozzle's upstream pressure was in the range of up to 2 bars.

Table 1. Summery of Experimental Conditions

Gas	Air
	Argon
	Helium
Liquid	Distilled water
	Sucrose solution (viscosity =5.38 mPa a)
	Sucrose solution (viscosity =10.5 mPa a)
	Ethanol (95%)
Nozzle diameter (mm)	1.07, 2.03, 2.85, and 4
Temperature (°C)	21–22

The height of liquid phase in the tank was kept constant at 0.30 m. The nozzle length was about 0.40 m and its immersion depth was 0.10 m, so that the distance from the nozzle tip to the bottom of the tank was 0.2 m. The nozzle distance from the tank walls was about 0.15 m to avoid any wall effects.

Preliminary measurements were taken with a fast video camera. It sampled at a frequency of 1000 Hz and with a resolution of 240 × 210 pixels.

A photodiode cell and a horizontal laser beam were used to measure jet penetration length, as shown in Figure 1. When the laser beam passes through the liquid to a photodiode cell, a voltage which depends on the intensity of the emergent beam is developed. The laser beam is greatly attenuated when it intersects with a gas–liquid interface and the voltage drops. For each gas flow rate, data were collected at different vertical distances from the nozzle tip in 2 mm increments. The photodiode cell was directly connected to a computer data acquisition system and data was acquired at 1000 Hz for 20 s.

Figure 2a shows 5 s of a typical raw photodiode signal for the case of air/sucrose-solution system with a viscosity of 10.5 mPa s at two different vertical distances (6 and 50 mm) below the nozzle tip. When the laser beam is near the nozzle tip (6 mm), it goes through two gas–liquid interfaces most of the time, and the average value of the signal is very small (about 1% of its maximum value). Further away from the nozzle tip (50 mm), the laser beam does not encounter gas jet or bubbles and the signal is very strong and stable. These two extreme conditions were used to calculate the fraction of time that gas jet was present in the path of the laser beam. This fraction of time translates to probability of gas jet presence at that particular condition. Table 1 summarizes experimental conditions.

Figures 2b, c show two intermediate cases for which, because the jet fluctuates, the beam may or may not cross gas–liquid interfaces. Figure 2b shows the signal at 30 mm from the nozzle tip, for which the presence of gas is more likely than for Figure 2c, for which the beam was 40 mm from the nozzle tip. Both Figures 2b, c show that, at these distances, the gas jet was not always present. This was confirmed by the fast video measurements.

From the average value of the signal obtained at a given distance, one can calculate the fraction of the time that the beam intersected with the gas jet, which corresponds to the probability that the jet is present at this location. It was found that 20 s of signal were sufficient for an accurate determination of the jet probability. Figure 3 shows that the jet probability decreases as the distance from the nozzle tip is increased. Three regions can be recognized, a region where the jet was practically always present, a region where the jet was never observed, and an intermediate region where the jet was sometime present.

The average jet penetration length ($L_{50\%}$) was taken to correspond to a 50% probability of jet presence and a four parameter sigmoid curve, fitted to the experimental data, was used for interpolation (see Figure 3). The span of the jet fluctuation range was taken as the differences between the

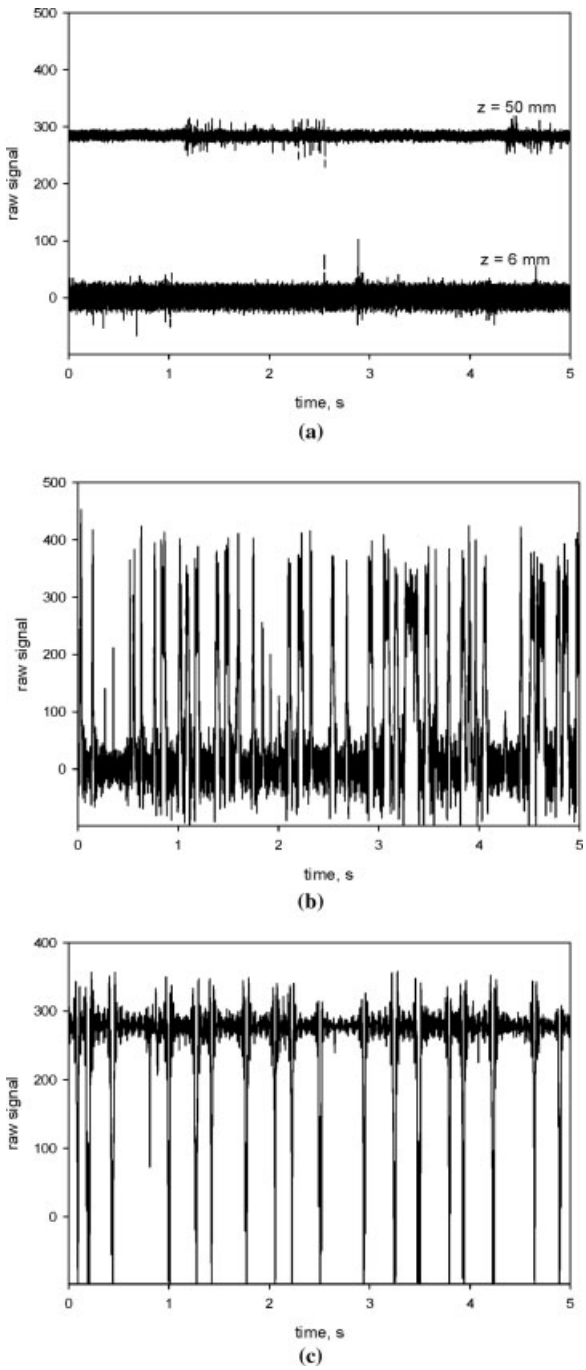

Figure 2. First 5 s of raw signals for air/sucrose solution system with liquid phase viscosity of 10.5 mPa s, d = 2.85 mm, and F_g = 0.3866 g/s.

(a) At 6 mm and 50 mm below nozzle tip. (b) At 30 mm below nozzle tip. (c) At 40 mm below nozzle tip.

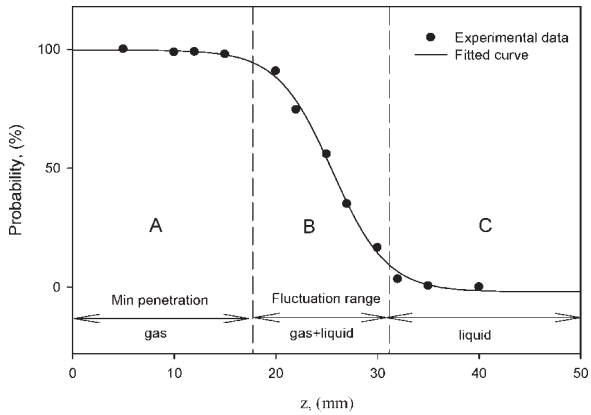

Figure 3. A sample graph of probability of gas jet presence vs. distance from nozzle tip for Air/sucrose solution with liquid viscosity of 10.5 mPa s and nozzle diameter of 2.85 mm, F_g = 0.265 g/s.

distances corresponding to 10 and 90% jet presence probabilities ($L_{10\%} - L_{90\%}$).

Flow Structure

Calculation of gas velocity at nozzle tip showed that subsonic flow occurs inside the tube (Ma $<$ 0.3). When gas injected to the liquid through a downward nozzle the whole process can be described as follow: the gas flow produces a bubble and bubble keeps growing until the buoyancy force gets strong enough to overcome inertial forces. At this point, bubble starts moving upward. Then bubble detaches from nozzle tip moving upward while covering nozzle tube. At low gas flow rates, a bubbling regime is dominant by increasing gas flow rate a fluctuation gas jet grows and bubble size increases. Figure 4 shows image of the flow at different gas flow rates.

Modeling

Flow structure of gas emerging from a downward submerged nozzle mainly depends on gas flow rate. By increasing gas flow rate, a transition between bubbling and jetting occurs. Bubble formation and rising were studied in details in the literature (Tsuge, 1986).[14] In the transition region and jetting regime, oscillations behavior was observed. The high-speed videos taken at different gas flow rate suggested that the cavity can be assumed as a downward cone.

Shell momentum balance

This model, which is based on a momentum balance, assumes a conical shape for the downward gas jet. Momentum input comes from the gas entering the control volume at the nozzle tip. Momentum output is negligible because of the low velocity of bubble leaving the control volume. The force acting on the control volume is the buoyancy force. The frictional force of the liquid on the control volume is negligible as the jet is assumed to be stationary (Figure 5).

The shell momentum balance for the cone is:

$$\sum F_z = \text{Momentum output} - \text{Momentum input} \tag{7}$$

The velocity of the gas bubbles where they leave the jet (i.e., the shell) is negligible and the exit momentum can, therefore, also be neglected.

$$\text{Momentum output} \approx 0 \tag{8}$$

The buoyancy force is:

$$\sum F_z = \rho_l V_{jet} g \approx \frac{\pi}{3} \rho_l g L_{jet}^3 \tan^2 \alpha \tag{9}$$

where V_{jet} is the gas jet volume and α is gas jet cone half-angle in equation. The input momentum can be calculated using the gas jet properties at the nozzle tip:

$$\text{Momentum input} = \frac{\pi d^2}{4} \rho_{tip} u_{tip}^2 \tag{10}$$

Substituting Eqs. 8, 9, and 10 into Eq. 7 gives:

$$\frac{\pi d^2}{4} \rho_{tip} u_{tip}^2 = \frac{\pi}{3} \rho_l g L_{jet}^3 \tan^2 \alpha \tag{11}$$

Rearranging the above equation gives:

$$\frac{L_{jet}}{d} = \left(\frac{0.75}{\rho_l g d \tan^2 \alpha} \right)^{\frac{1}{3}} \left(\rho_{tip} u_{tip}^2 \right)^{\frac{1}{3}} \tag{12}$$

The first term shows the effects of liquid density and nozzle diameter and the second term shows the effect of the momentum flux at the nozzle tip, which is a function of gas flow rate, gas density and nozzle diameter.

The same equation can also be written with a modified Froude number:

$$\frac{L_{jet}}{d} = 0.9086 (\cot \alpha)^{\frac{2}{3}} (Fr)^{\frac{1}{3}} \tag{13}$$

where:

$$Fr = \frac{\rho_{tip}}{\rho_l} \frac{u_{tip}^2}{gd} = \frac{1}{\rho_{tip}} \frac{\left(\rho_{tip} u_{tip} \right)^2}{\rho_l g d} \tag{14}$$

The liquid density, the distance, and the mass velocity of the gas are usually known. This equation, however, also requires the knowledge of the gas density at the nozzle tip, which must usually be predicted (see Appendix A).

The nozzle behaves as an orifice and a higher flow rate requires a higher pressure drop at the nozzle tip ($P_{tip} - P_{atm}$). Since P_{atm} is constant, P_{tip} has to increase to provide enough driving force for higher gas flow rates. Experiments were performed to measure P_{tip} for different gases. As explained in the appendix, two small tubes with same diameter of nozzle and different lengths were used to estimate the gas pressure at the nozzle tip. Upstream pressures (P_{a1}, P_{a2}) were recorded at the same gas flow rate for each case. Then, the ideal gas law was used to calculate the gas density at the nozzle tip. Results are shown in Figure 6 for a nozzle dia-

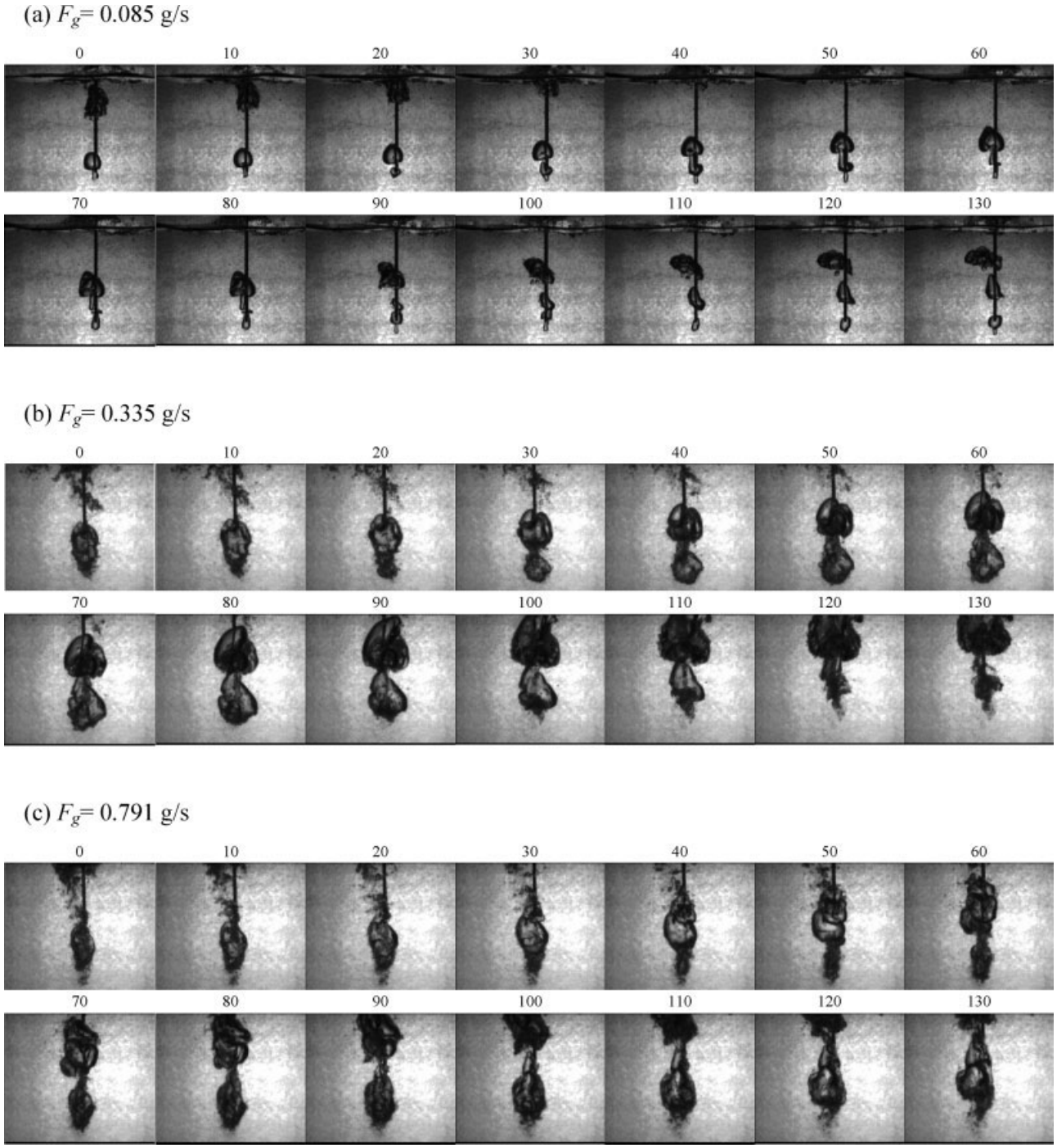

Figure 4. Downward gas jet for Air/water system and nozzle diameter of 2.85 mm at 20°C and gas flow rate of (a) 0.085 g/s, (b) 0.335 g/s, and (c) 0.791 g/s, numbers shows time in ms.

meter of 2.85 mm at room temperature (20°C) for three different gases. The gas density at nozzle tip increases slightly as the gas flow rate increases.

One can then calculate gas jet penetration by using Eq. 13 if the cone half angle (α) is known. Analyzing videos taken by the high-speed camera shows that at higher gas flow rates the jet half-angle is between 8 and 13°. An average value of 10° will be used in this model. Considering this value for α Eq. 13 can be simplified:

$$\frac{L_{\text{jet}}}{d} = 1.424(Fr)^{\frac{1}{3}} \tag{15}$$

Results and Discussion

Effect of gas velocity and nozzle diameter

The dimensionless jet penetration length obtained by dividing the average jet penetration length ($L_{50\%}$) by the nozzle diameter was used to study the effect of design and physical properties of

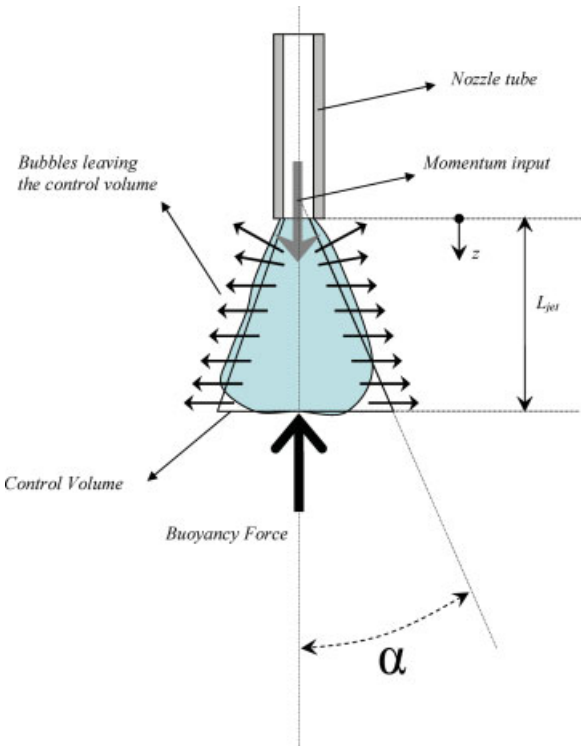

Figure 5. A model for downward gas jet in liquid.

[Color figure can be viewed in the online issue, which is available at www.interscience.wiley.com.]

both phases. Generally increasing gas flow rate provides more kinetic energy to the jet and increases the jet penetration length. $L_{50\%}/d$ was found to be nearly independent of the nozzle diameter, for a given gas velocity at the tip. It means more gas flow rate needed for larger diameters to have the same dimensionless penetration length. Gas velocity at nozzle tip was calculated by using gas density at nozzle tip which is calculated in Appendix A. One explanation would be that also it was found that $L_{50\%}/d$ vs. gas mass flow rate can be expressed as a power law function for each nozzle diameter with higher power for smaller nozzle diameters. Figure 7 shows that, for the air–water system, the

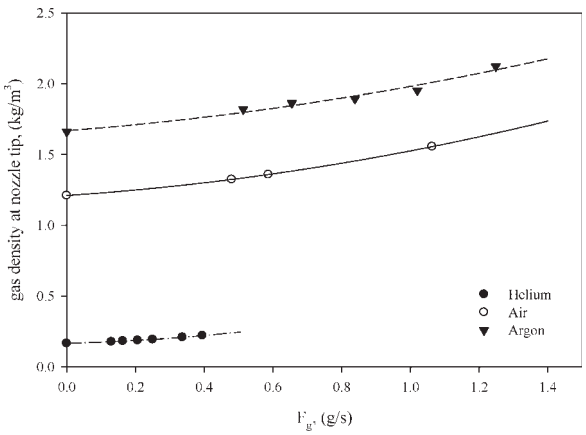

Figure 6. Gas density at nozzle (0.70 m length and 2.85 mm ID) tip for a downward gas jet of air, argon and helium at 20°C.

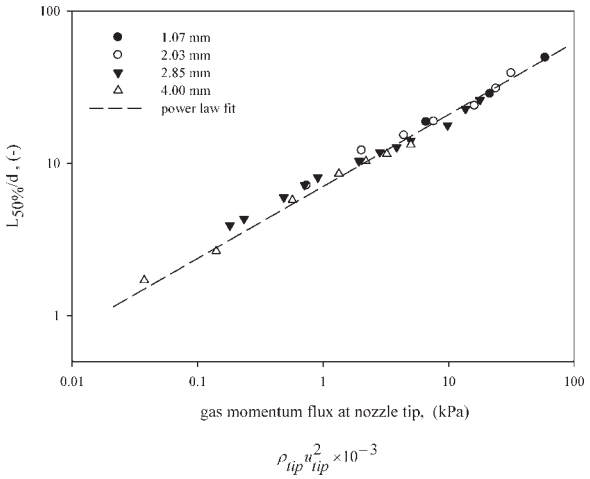

Figure 7. Downward gas jet penetration length data for air/water system at 20°C and different nozzle diameters vs. gas momentum flux at nozzle tip.

dimensionless jet penetration ($L_{50\%}/d$) can be correlated with a power law function of the jet momentum flux at the nozzle tip.

Effect of gas properties

Three gases were studied: helium, argon, and air. Because of lower molecular weight of helium, large volumetric flow rates and high jet velocities can be obtained even at small mass flow rates. It was found that a gas with lower molecular weight (helium in this case) has higher penetration length than gas with higher molecular weight at same gas mass flow rate and same nozzle diameter. Figure 8 summarizes all experimental data for the three gases in a unified and compact form in terms of the gas momentum flux ($\rho_{\text{tip}} u_{\text{tip}}^2$). Since all data can be fitted with a power law expression of the gas momentum flux, the main effect of the gas molecular weight is to change the momentum flux by changing the expansion pressure drop and, hence, the density at the nozzle tip.

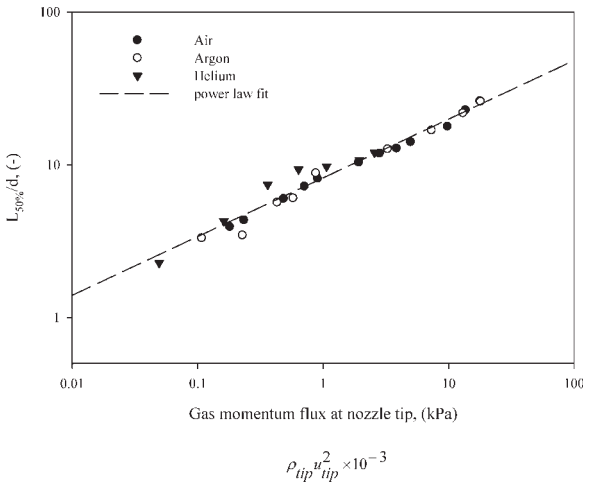

Figure 8. Effect of gas density on gas jet penetration length for clear water and different gases and nozzle diameter of 2.85 mm at 20°C vs. gas momentum flux.

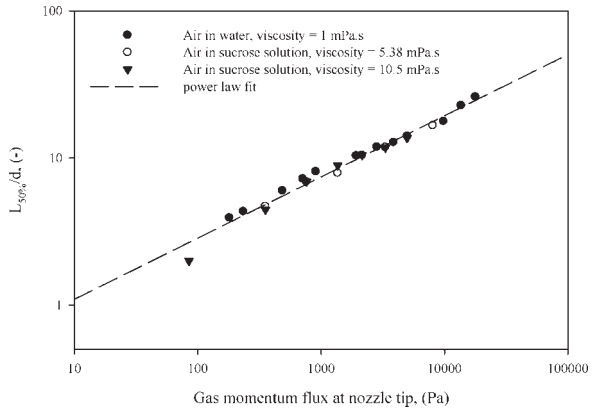

Figure 9. Effect of liquid phase viscosity on gas jet penetration length for air/sucrose solutions with different viscosities and nozzle diameter of 2.85 mm at 20°C vs. gas momentum flux.

Effect of liquid viscosity

Sucrose solutions were prepared at different concentrations and their viscosities were measured at 20°C, that is, at the same temperature as the experiments. Liquids with a viscosity ranging from 1 to 10.5 mPa s were studied. Figure 9 shows that the liquid viscosity has nearly no effect on jet penetration length in this range.

Effect of liquid surface tension

Figure 10 shows that the liquid phase surface tension has no detectable effect at low gas flow rates. At higher gas flow rates, when gas momentum flux is greater than 5000 Pa, the gas jet penetrates slightly less in a liquid with a larger surface tension. Increasing the surface tension means that more energy is required to create a certain amount of new surface area and less energy is available for penetration.

General correlation of gas jet penetration in liquid phase

Figure 11 shows that all experimental data, including various gas/liquid systems and nozzle diameters, can be predicted with a rather good accuracy with a power law expression of the dimensionless group of $\frac{\rho_{tip}u_{tip}^2}{\rho_l g d}$ at the nozzle tip. This correlation was compared with other correlation later. The power is close to theoretical value of 0.3333.

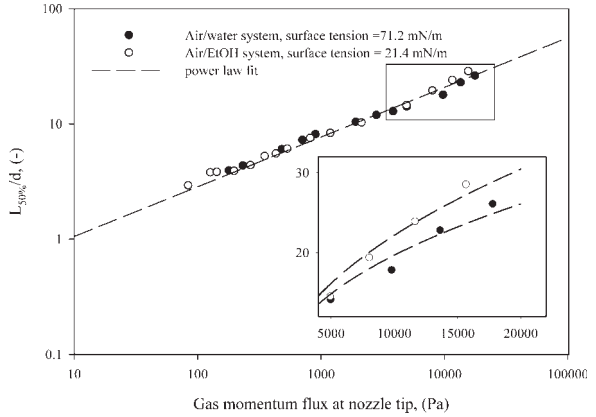

Figure 10. Effect of liquid phase surface tension on gas jet penetration length for air/water and air/ethanol systems and nozzle diameter of 2.85 mm at 20°C vs. gas momentum flux.

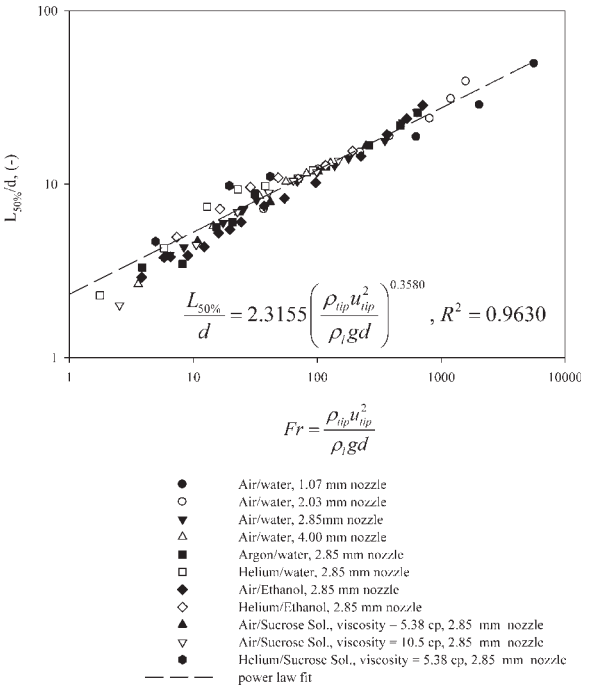

Figure 11. Downward gas jet penetration length for various gas/liquid systems and different nozzle diameters at 20°C (all experimental data in one graph).

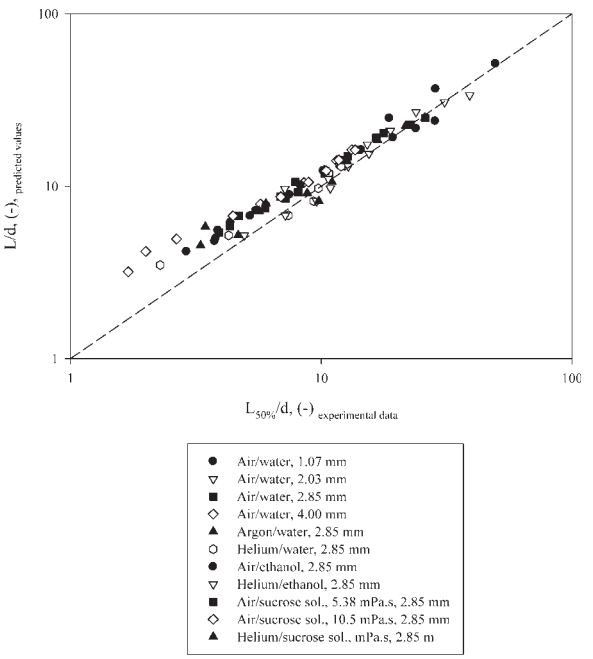

Figure 12. Comparison of shell momentum balance model (Eq. 15) with experimental gas jet penetration data of various gas/liquid systems and different nozzle diameters at 20°C.

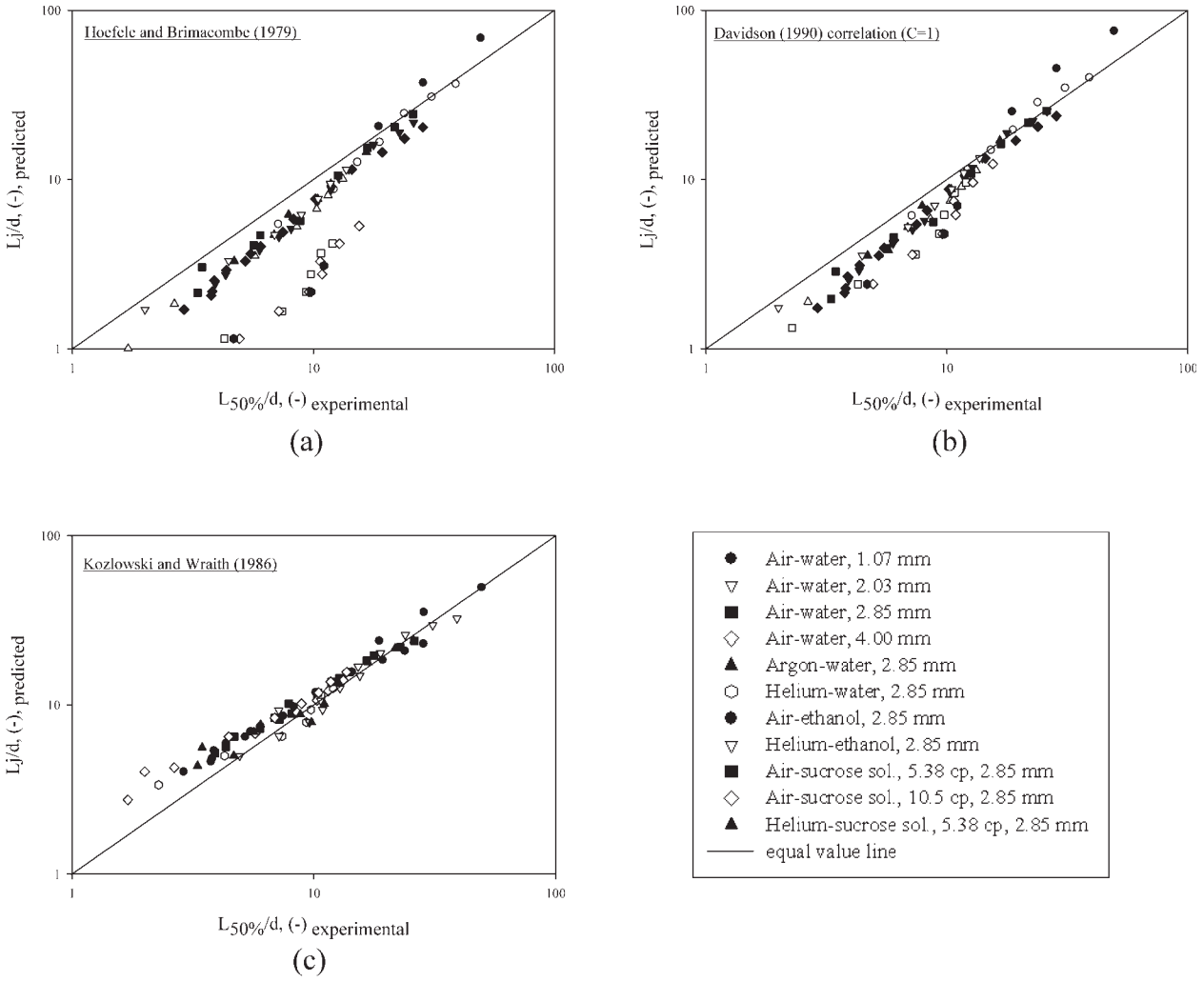

Figure 13. Comparison of experimental data with three available correlations:

(a) Hoefele and Brimacombe (1979)[11], (b) Davidson (1990)[12] ($C = 1$), (c) Kozlowski and Wraith (1986)[13].

$$\frac{L_{50\%}}{d} = 2.3155\left(\frac{\rho_{\text{tip}} u_{\text{tip}}^2}{\rho_l g d}\right)^{0.3580} \tag{16}$$

Shell momentum balance model

Figure 12 shows how the predictions from the new simple model, presented in section 3, fit to the experimental data. At higher penetration lengths, which correspond to higher gas flow rates, there is good agreement between experimental data and predicted values. At low penetration lengths, however, the predicted value is much higher than the measured penetration length. The reason for this is at lower gas flow rates, there is no gas jet and bubbling occurs directly at the nozzle tip.

Comparison with other correlations

Comparison has been made between our experimental data and the correlations available from the literatures that were reviewed in the introduction section. Some correlations are for horizontal jets and some are for high pressure conditions. Figures 13 shows how the predictions of these correlations compared with the measured jet penetrations of this study. The correlation from Hoefele and Brimacombe (1979)[11], which was developed for horizontal gas jets, failed and especially with helium gas data (see Figure 13). The correlation from Davidson (1990)[12] shows a fair agreement at higher penetration lengths. The corrected correlation from Kozlowski and Wraith (1986)[13] by using gas density at nozzle tip condition gives better results at higher penetration lengths. Table 2 shows summation of error squares for all correlations including corrected Kozlowski and Wraith (1986)[13] by using gas density at nozzle tip condition and shell momentum balance model.

Jet fluctuation frequency

The gas jet fluctuation frequency was measured by filtering out frequencies above 45 Hz to eliminate electrical noise and using cycle analysis (Briens, 2002)[15]. Cycle analysis uses *V*-statistics which is based on Hurst analysis. It is used to detect regular cycle's time of the raw signals. Gas jet fluctuation frequency was calculated using this cycle time. This is

Table 2. Comparison of Correlations and Shell Momentum Balance Model

Correlation or Model	Hoefele and Biomacombe (1979)[11]	Davidson (1990)[12]	Shell Momentum Balance model	Kozlowski and Wraith (1986)*[13]	Corrected Kozlowski and Wraith (1986)†[13]	This Work
Summation of error squares	1667.7	8469.5	525	511.1	293.7	175

*Gas density was calculated at room temperature and pressure.
†Gas density was calculated at room temperature and nozzle tip pressure.

validated later by comparison of the optical technique data. Figure 14 shows that the jet fluctuation frequency reaches a maximum value at a certain distance from the nozzle tip for each specific experimental condition. This distance was found to correspond to the average penetration length, $L_{50\%}$. These two techniques are compared in the next section. This is also the distance at which the average amplitude of the signal fluctuations, as quantified by the standard deviation of the signal, is greatest. Figure 14 shows that, in this case, the maximum frequency was about 8.5 Hz.

Figure 15a shows how the maximum fluctuation frequency varied with experimental conditions for the air/water system and different nozzle diameters. The maximum fluctuation frequency generally decreased with increasing gas flow rates. Decreasing the gas jet fluctuation frequency is in agreement with theoretical equation of Kozlowski and Wraith (1986).

$$f = \frac{g^{3/5}}{1.45 Q_g^{1/5}} \tag{17}$$

where f is the fluctuation frequency (Hz) and Q_g is the volumetric gas flow rate (m^3/s). This trend is very clear for the nozzle diameter of 4 mm which creates a larger gas jet. Increasing the gas flow rate will increase gas jet penetration length and gas jet volume. So at higher flow rates, a larger amount of liquid has to be displaced for each pulse. Since liquid inertia is proportional to mass of liquid, it is harder to displace a large amount of liquid than a small amount. Figure 15b shows that the maximum fluctuation frequency is affected by the liquid viscosity. Frame by frame analysis of high-speed videos showed that the gas jet penetration length fluctuated widely with a frequency ranging from 8 to 14 Hz.

Using jet fluctuation frequency to determine average penetration length

The average gas jet penetration can also be taken as the distance from the nozzle tip where the fluctuation frequency reaches to a maximum value (Figure 14). Figure 16 shows that there was a very good agreement between the jet penetration obtained from the frequency and the penetration, used earlier, which was obtained from the distance at which the

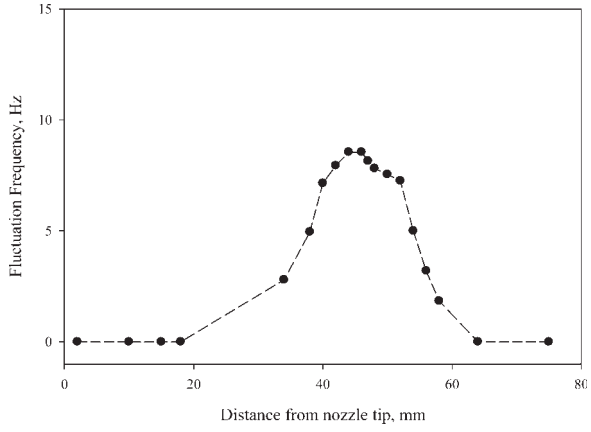

Figure 14. Fluctuation frequency of downward gas jet for air/water system and nozzle diameter of 4 mm and gas flow rate of 49.8 g/min at 20°C.

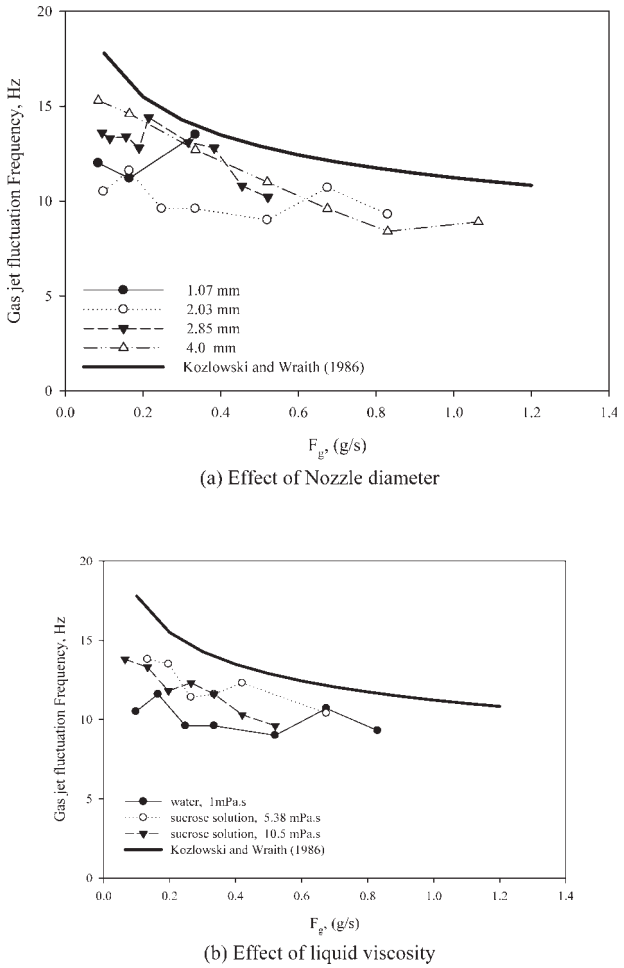

Figure 15. Gas jet fluctuation frequency at 20°C.

(a) Effect of nozzle diameter and gas flow rater for air/water system. (b) Effect of liquid viscosity and gas flow rate for nozzle diameter of 2.03 mm.

jet presence probability was 50%. Analysis of high-speed videos, for a few test cases, confirmed these results.

Average bubble size

The average bubble size was calculated from the maximum jet fluctuation frequency and the gas volumetric flow rate at the nozzle tip conditions.

$$V_B = \frac{Q_g}{f} \tag{18}$$

Figure 17 shows how the diameter of the bubbles formed from the jet varied with the gas flow rate. It shows that the nozzle diameter, gas, and liquid properties had no significant effect on this bubble size. Davidson and Harrison (1963)[16] proposed a well-known correlation for the initial bubble volume for upward nozzles, using an analysis of the forces during bubble formation and detachment from the nozzle tip. Our results show that, for downward nozzles, the bubble diameter is 35–47% higher than predicted by for upward nozzles (Figure 17). Please note that the gas volumetric flow rate is expressed at the downstream or liquid tank pressure as specified by Davidson and Harrison. One possible explanation is that bubbles from downward jets have more time to grow before detachment due to the downward momentum of the gas flowing from the nozzle tip. The correlation for the initial diameter of bubbles formed with downward nozzles is:

$$d_B = 0.5238\, Q_g^{0.3753}, \quad R^2 = 0.9759 \tag{19}$$

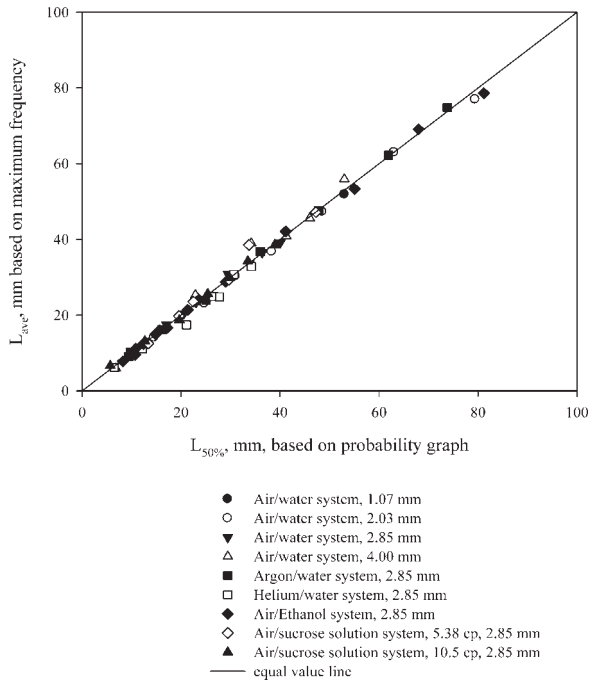

Figure 16. Comparison of two experimental techniques of various gas/liquid systems and different nozzle diameters at 20°C.

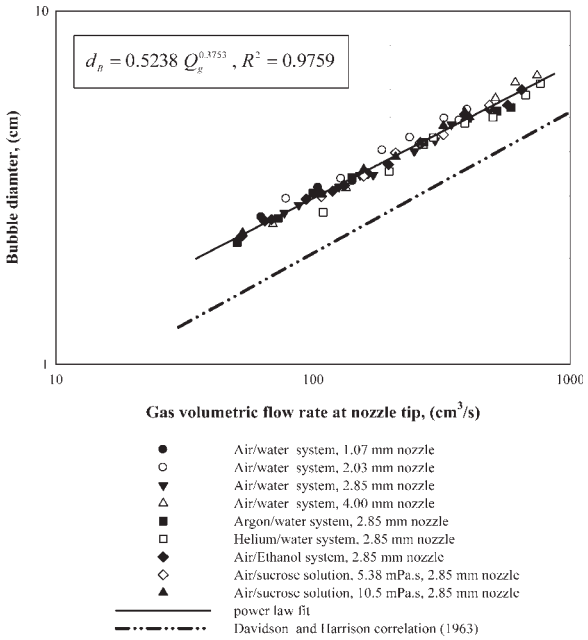

Figure 17. Bubble diameter for different gas/liquid systems and different nozzle diameters at 20°C based on jet fluctuation frequency.

Jet fluctuation behavior

Figure 6b shows the fluctuation behavior of the gas jet for the Air/water system and gas flow rate of 0.335 g/s. A rough estimate of jet fluctuation frequency can be made using high-speed videos. If birth of bubbles is considered as a cycle, one can see that it takes about 120 ms to grow and move up from the tip of the nozzle where a new bubble is going to be born (first bubble born at 10 ms and second bubble 130 ms). Frequency corresponds to this time interval is 8.3 Hz. The signal analysis technique gives 9 Hz for this condition. So there is an agreement between optical technique and signal analysis.

Conclusion

The penetration of downward gas jets in liquid phase was studied using optical technique at subsonic conditions. Liquid viscosity has almost no effect at this range (up to 10.5 mPa s). Also results showed that gas jet penetration increases slightly with decreasing liquid phase surface tension at higher flow rates (for a gas momentum flux at nozzle tip $>$ 5000 Pa).

Effects of nozzle diameter, gas mass flow rate, liquid and gas properties can be expressed using a power law equation in terms of gas momentum flux at nozzle tip. A simple shell momentum balance gives good predictions of the jet penetration in the jetting range, which is in agreement with the previous correlation provided by Kozlowski and Wraith (1986)[13] when the gas density at nozzle conditions is used.

The fluctuation frequency of the gas jet varied between 8 and 14 Hz depending on the gas flow rate. The fluctuation frequency decreases with increasing gas flow rate. The gas bubble size can be estimated from the fluctuation frequency and the bubble volume for a downward gas jet is almost 2–3

times larger than the volume predicted with the correlation from Davidson and Harrison for upward jets.

Notation

A = area, m^2
C_p = liquid specific heat, J/kg K
d = nozzle inner diameter, m
f = gas fluctuation frequency, Hz
F_g = gas mass flow rate, g/s
F_z = vertical acting force on gas jet, N
Fr^* = modified Froude number, dimensionless (Eq. 2)
Fr = modified Froude number, dimensionless (Eq. 4)
g = acceleration caused by gravity, 9.81 m/s^2
G_m = average gas mass flux at gas liquid interface, kg/m^2 s
h_{fg} = heat of vaporization of liquid, J/kg
L = average gas jet penetration length, m
Ma = Mach number
M_W = gas molecular weight, g/mole
P = gas pressure, Pa
P_{a1}, P_{a2} = upstream gas pressure, Pa
Q_g = gas volume flow rate at nozzle tip, cm^3/s
R = universal (ideal) gas constant, 8.314472 J/ (K mol)
T = temperature, K
T_∞ = liquid bath temperature, K
T_s = steam temperature, K
u = gas velocity, m/s
V = volume of control volume, cm^3
V_B = bubble volume, cm^3
z = distance from nozzle tip, downward direction, m
Z_1, Z_2 = length of tube, m

Greek letters

α = gas jet cone half-angle in Eq. 8, radians
β = constant in Eq. 16
γ = power in Eq. 16
λ = pressure drop due to friction per unit length, Pa/m
ρ = density, kg/m^3

Subscripts

l = liquid
g = gas
tip = properties evaluated at conditions of the tip of the nozzle
atm = properties evaluated at atmospheric pressure
jet = jet properties
j,max = maximum jet penetration length in Eq. 6
50% = average jet penetration length calculated based on 50% of probability of gas presence
90% = minimum jet penetration length calculated based on 90% of probability of gas presence
10% = maximum jet penetration length calculated based on 10% of probability of gas presence

Literature Cited

1. Emami A, Briens CL. A method for the detection of defluidized zones in slurry bubble columns. *Can J Chem Eng*. 2003;81:451–455.
2. Merry JMD. Penetration of a horizontal gas jet into a fluidized bed, *Trans Instn Chem Engrs*. 1971;49:189–195.
3. Merry JMD. Penetration of vertical jets into fluidized beds, *AIChE J*. 1975;21:507–510.
4. Musmarra D. Influence of particle size and density on the jet penetration length in gas fluidized beds. *Ind Eng Chem Res*. 2000;39:2612–2617.
5. Okhotskii VB. Depth of penetration of a gas jet into a granular medium. *Theor Foundations Chem Eng*. 2001;35:199–200.
6. Vaccaro S. Analysis of the variables controlling gas jet expansion angles in fluidized beds. *Powder Technol*. 1997;92:213–222.
7. Vaccaro S, Musmarra D, Petrecca M. Evaluation of the jet penetration depth in gas-fluidized beds by pressure signal analysis. *Int J Multiphase Flow*. 1997;23:683–698.
8. Zenz FA. Bubble formation and grid design. I. *Chem E Symp Ser*. 1968; No. 30:136–139.
9. Kerney PJ, Faeth GM, Olson DR. Penetration characteristics of a submerged steam jet. *AIChE J*. 1972;18:548–553.
10. Carreau JL, Roger F, Loukarfi L, Gbahoue L, Hobbes Ph. Penetration of a horizontal gas jet submerged in a liquid. Proceedings of the 21st Intersociety Energy Conversion Engineering Conference 1986;1:315–319, San Diego, California, August 25–29.
11. Hoefele EO, Brimacombe JK. Flow regimes in submerged gas injection. *Metall Metals Trans B*. 1979;10B:631–648.
12. Davidson MR. Flow in the stagnation zone during submerged injection of a swirling gas jet. *Chem Eng Sci*. 1990;45:687–694.
13. Kozlowski MA, Wraith AE. Jet cavity at submerged vertical lance. *Ironmaking steelmaking*. 1986;13:190–194.
14. Tsuge H. Hydrodynamics of bubble formation from submerged orifice. In: Cheremisinoff, editor. *Encyclopedia of Fluid Mechanics*. Houston, TX: Gulf Publishing Corporation, 1986:191–232.
15. Briens LA, Briens CL. Cycle detection and characterization in chemical engineering. *AIChE J*. 2002;48:970–980.
16. Davidson JF, Harrison H. *Fluidized Particles*. Cambridge: Cambridge University Press, 1963.

Appendix A: Estimation of the Gas Density at the Nozzle Tip

The gas density at nozzle tip can be estimated from the pressure at the tip, using the ideal gas law. The pressure at nozzle tip is calculated from the predicted pressure drop through the nozzle.

Experimental measurement showed that gas flow in the nozzle can be considered as subsonic and incompressible flow with reasonable approximation (Ma < 0.3). So, gas density at the nozzle tip is equal to gas density at upstream condition approximately ($\rho_{tip} \approx \rho_{a1}$). Substation this in the mass balance equation we get: $u_{tip} \approx u_{a1}$ (please note that cross sectional area is constant). So it means that pressure drop per unit length is approximately same in the entire length of the tube ($\frac{dP}{dL} \approx$ constant). This allows us to estimate pressure drop through the tube length by measuring pressure drop in a small length of the same tube at the same flow conditions. Finally, by knowing pressure drop and upstream pressure one can calculate gas pressure at the nozzle tip.

Experiments were, first, conducted to obtain the gas pressure drop over a small length of the tubing used for the nozzles. Two different tube lengths were used and the upstream pressures (P_{a1}, P_{a2}) were measured in open air for each gas flow rate.

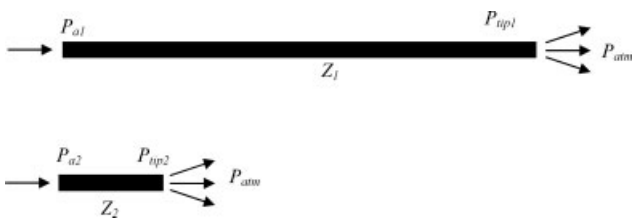

For the same flow rate, we have:

$$\frac{P_{a1} - P_{\text{tip1}}}{Z_1} = \frac{P_{a2} - P_{\text{tip2}}}{Z_2} = \lambda = \text{pressure drop due to friction per unit length} \quad \text{(A1)}$$

$$P_{\text{tip1}} - P_{\text{atm}} = P_{\text{tip2}} - P_{\text{atm}} = \text{pressure lost due to expansion at nozzle tip} \quad \text{(A2)}$$

$$P_{\text{tip1}} = P_{\text{tip2}}, \quad P_{\text{a1}} - P_{\text{tip1}} = \lambda Z_1, \quad P_{\text{a2}} - P_{\text{tip2}} = \lambda Z_2 \quad \text{(A3)}$$

$$\lambda = \frac{P_{\text{a1}} - P_{\text{a2}}}{Z_1 - Z_2}, \quad \text{(A4)}$$

$$P_{\text{tip1}} = P_{\text{a1}} - \lambda Z_1 = P_{\text{a1}} - \frac{P_{\text{a1}} - P_{\text{a2}}}{Z_1 - Z_2} Z_1 \quad \text{(A5)}$$

Measuring the upstream pressure at same flow rate for different tube lengths, therefore, allows the prediction of the gas pressure at the nozzle tip. The ideal gas law can, then, be applied:

$$\rho_{\text{tip}} = \frac{P_{\text{tip}} MW}{RT} \quad \text{(A6)}$$

Figure 8 shows effect of gas flow rate on gas density at nozzle tip.

Manuscript received Jan. 2, 2007, and revision received Mar. 5, 2008.